



Ruthenium nanoparticles supported on magnesium oxide: A versatile and recyclable dual-site catalyst for hydrogenation of mono- and poly-cyclic arenes, N-heteroaromatics, and S-heteroaromatics



Minfeng Fang, Roberto A. Sánchez-Delgado*

Chemistry Department, Brooklyn College and The Graduate Center, The City University of New York (CUNY), 2900 Bedford Avenue, Brooklyn, NY 11210, United States

ARTICLE INFO

Article history:

Received 4 November 2013

Revised 23 December 2013

Accepted 30 December 2013

Available online 29 January 2014

Keywords:

Hydrogenation

Ru nanoparticles

Magnesium oxide

Hydrogenation

Aromatics

N-heteroaromatics

S-heteroaromatics

Heterolytic hydrogen splitting

Ionic hydrogenation mechanism

Dual-site

ABSTRACT

The development of catalysts capable of promoting hydrogenation of aromatics while being resistant to poisoning by nitrogen- and sulfur-containing species is of much interest in connection with hydrotreating of fossil fuels. We report a catalyst composed of ruthenium nanoparticles supported on magnesia, designed to promote heterolytic hydrogen splitting and surface ionic hydrogenation pathways. The catalyst, prepared through a one-pot procedure, promotes the hydrogenation of mono- and poly-cyclic arenes, as well as N- and S-heteroaromatics representative of fossil fuels components. Of particular significance are the superior activity and wider substrate scope of the catalyst, in relation to other known supported noble metals, and the excellent recyclability and long catalyst lifetime. Based on our experimental data, a dual-site catalyst structure and an associated dual-pathway mechanism are proposed, which may have interesting implications for the development of new poison-tolerant noble metal catalytic systems.

© 2014 Elsevier Inc. All rights reserved.

1. Introduction

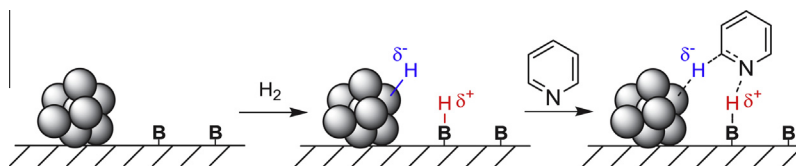
Fossil fuels—coal, oil and natural gas—currently provide over 80% of the energy consumed in the US [1] and will continue to be the predominant energy source worldwide by 2035 [2,3], in spite of the aggressive development of alternative renewable energy sources. In particular, global consumption of conventional transportation fuels, a significant source of air pollution, will continue to grow. Environmental regulations impose increasingly severe restrictions on the aromatics, sulfur, and nitrogen content allowed in fuels [4–7]; the low levels required are difficult to achieve with current refining technologies. Considering the current level of oil consumption, in the foreseeable future, liquid fuels will necessarily come from unconventional sources, such as heavy and extra-heavy oil and bitumen deposits. Such fossil materials contain higher levels of poly-cyclic aromatics, nitrogen and sulfur, all of which need to be removed or transformed to produce cleaner fuels and to avoid poisoning of precious metal catalysts employed in subsequent steps of the refining process [8,9].

Catalytic hydrogenation plays a pivotal role in the manufacture of cleaner fuels: the proportion of aromatic hydrocarbons is lowered through hydrogen addition (HYD); removal of nitrogen and sulfur is routinely achieved through hydrodenitrogenation (HDN) and hydrodesulfurization (HDS), both of which involve key hydrogenation steps within complex reaction networks [8,10]. Conventional metal sulfide hydrotreating catalysts (Co–Mo, Ni–Mo, and Ni–W) can only saturate a moderate proportion of aromatics due to thermodynamic equilibrium limitations under typical operating conditions (300–400 °C, 50–100 atm) [8]. Supported noble metal catalysts, on the other hand, can function at lower temperatures far from equilibrium conditions, but they are easily poisoned by N- and S-containing compounds present in refinery feeds [11]. Therefore, there is a continuing need for efficient catalysts capable of promoting hydrogenation of aromatics under moderate reaction conditions, while being resistant to poisoning by nitrogen and sulfur species.

Although hydrogenation by metals is a well-developed field [12–14], the use of nanoparticles (NPs) in catalysis has been attracting increasing interest due to the advantageous activity and selectivity features associated with the small particle size [15–26]. Ruthenium nanoparticles (RuNPs) in particular, stabilized by ligands or macromolecules [27–35], surfactants [33,36], ionic

* Corresponding author. Fax: +1 718 951 4607.

E-mail address: Rsdelgado@brooklyn.cuny.edu (R.A. Sánchez-Delgado).



Scheme 1. Heterolytic H_2 activation and ionic transfer to polar unsaturated bonds on a solid catalyst surface comprising metal NPs and basic functionalities (B) on the support.

liquids (ILs) [37–41], or supports [42–67], have been employed for hydrogenation of aromatics, mostly of benzene and other monocyclic arenes. The role of the solid supports, in most instances, is to avoid NP aggregation and to facilitate catalyst recovery and recycling, but seldom to intervene directly in the chemistry of key steps of the reaction.

The most widely accepted hydrogenation mechanisms on solid metal-containing catalysts involve homolytic H_2 splitting on surface metallic sites into hydrogen atoms, which are subsequently transferred to the chemisorbed substrates [12,14]. N- or S-containing species frequently bind strongly to such active metal sites, causing catalyst deactivation or poisoning. An interesting but much less frequently encountered alternative pathway is the base-assisted heterolytic splitting of hydrogen into H^- and H^+ , followed by outer sphere ionic transfer to polar unsaturated bonds of the substrate (Scheme 1). Hydrogenation mechanisms of this type do not require the direct binding of substrates or products to the metallic sites, thereby opening a possibility to avoid poisoning. Heterolytic hydrogen activation and ionic hydrogenation routes are well established in solution chemistry, e.g. Noyori's mechanism [68], but they remain largely unexplored on solid catalysts, although such reaction pathways have been suggested to occur on metal sulfides [69] or ceria-supported gold catalysts [70], with surface sulfur or oxygen sites acting as the proton acceptors, respectively.

Our working hypothesis is that a surface nanostructure composed of small metallic particles immobilized on a support that is rich on basic sites can promote heterolytic hydrogen splitting and ionic hydrogenation mechanisms through a metal-support bifunctional effect. Hydrogenase enzymes operate through similar bifunctional pathways with heterolytic H_2 activation taking place at a metal site in tandem with a basic sulfur atom from a neighboring cysteine moiety, to produce two protons and two electrons [71]. In line with our hypothesis, we have shown that a material composed of RuNPs supported on a poly(4-vinylpyridine) resin (Ru/PVPy) is a versatile catalyst for the hydrogenation of mono- and poly-nuclear arenes and N-heteroaromatic compounds. Detailed mechanistic studies led us to propose a dual-site, substrate-dependent hydrogenation cycle involving ionic pathways for N-heterocyclic substrates [72]. Alkaline earth metal oxides bear abundant highly basic surface oxygen sites, and therefore, they should be superior to PVPy as NP supports. Magnesium oxide in particular has been employed as a basic catalyst for a variety of organic reactions [73,74]; heterolytic H_2 dissociation into H^+ and H^- was claimed to occur over $Mg^{2+}-O^{2-}$ pairs on the MgO surface during hydrogenation and amination of conjugated dienes [75]. We reasoned that depositing noble metal NPs on MgO surfaces would enhance the activity and expand the scope of hydrogenation reactions, since noble metals are good hydride carriers and their combination with surface O atoms can create the metal-base bifunctional sites envisaged in our design for heterolytic H_2 activation and ionic hydrogenation pathways.

Here, we report a new catalyst composed of RuNPs on MgO (Ru/MgO), which promotes the liquid-phase hydrogenation of mono- and poly-nuclear aromatic hydrocarbons, N-heteroaromatics, and S-heteroaromatics. This Ru/MgO material displays enhanced

efficacy and substrate versatility in relation to the Ru/PVPy [72] and Pd/MgO [76] systems described by us before. Specifically, Ru/MgO is highly active for hydrogenation of mono- and poly-nuclear aromatic hydrocarbons and N-heteroaromatics under mild conditions; it can also hydrogenate S-heteroaromatics at higher temperatures. Mechanistic studies suggest the existence of two different types of active sites on Ru/MgO, associated with a dual mechanism. Other magnesia-supported ruthenium catalysts have been reported for NO reduction [77,78], transfer hydrogenation of carbonyl compounds [79], and ammonia synthesis [80–83], but to our knowledge, no examples are available for hydrogenation of aromatic compounds.

2. Results and discussion

2.1. Synthesis of Ru/MgO catalysts

The Ru/MgO catalysts were prepared by $NaBH_4$ reduction of $RuCl_3 \cdot 3H_2O$ in methanol under nitrogen at room temperature in the presence of suspended MgO, previously calcined at 500 °C in the air for 2 h. The formation of RuNPs and their attachment to the support can be visualized by the rapid discoloration of the solution and the darkening of the solid; the absence of any bands in the UV–vis spectrum of the final solution, other than those ascribed to the solvent, indicates that reduction of the metal salt to metallic Ru was complete. The lack of hydrogenation activity of the filtrate, together with EDX analysis of the solid described below, confirms that no suspended nanoparticles remain in the liquid phase and that all the metal is attached to the support. The catalysts were routinely stored under nitrogen but weighed quickly in the air prior to use. Three materials with a nominal Ru content of 1 wt%, 5 wt%, and 10 wt% were prepared using commercial MgO powder. An analogous catalyst with a nominal 5 wt% Ru loading was synthesized through the same procedure but using a MgO powder (denoted as MgO*) prepared by the sol–gel method with $MgCl_2$ (aq.) and NaOH (aq.) and calcination of the resulting $Mg(OH)_2$ at 500 °C in the air for 2 h.

2.2. Structure, texture, and composition of Ru/MgO catalysts

The Ru/MgO catalysts appear as fine gray to black powders depending on the metal loading. Transmission electron microscopy (TEM) images of the catalysts reveal the presence of highly dispersed RuNPs on the MgO support with mean diameters of 1.5, 1.8, and 2.1 nm for the 1 wt%, 5 wt%, and 10 wt% catalysts, respectively (see Figs. 1 and S1). Fig. 1a shows an image of a freshly prepared 5 wt% catalyst, and Fig. S1 contains images for fresh 1 wt% and 10 wt% catalysts. The average particle size is practically independent of the metal loading, with the majority of particles falling within the narrow range 1–3 nm, as can be appreciated in the size distribution histograms.

The average particle size and size distribution of 5 wt% Ru/MgO remain essentially unchanged after a quinoline hydrogenation run performed at 150 °C and 50 atm for 2 h (Fig. 1b), indicating that no sintering or other aggregation processes take place under typical

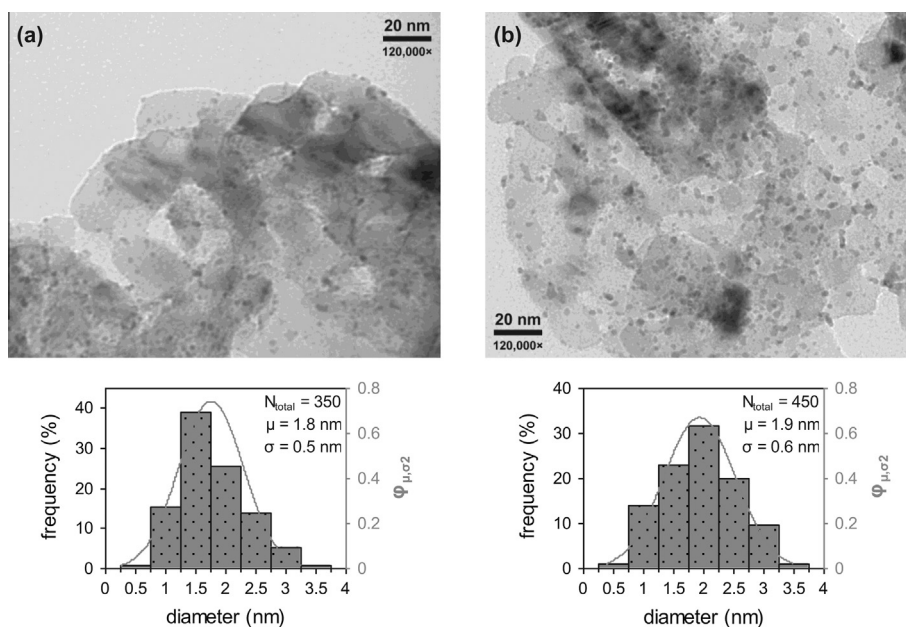


Fig. 1. Transmission electron micrographs of samples of (a) a freshly prepared and (b) a used 5 wt% Ru/MgO catalyst with RuNPs size distribution histograms and normal distribution curves.

hydrogenation conditions. To identify the crystalline structure of RuNPs on MgO surface, a TEM image at high magnification (500,000 \times) was obtained for a 10 wt% catalyst sample (Fig. S2). Lattice fringes were observed on a particle with a spacing of 2.3 Å (1.17 nm for 5 consecutive fringes), which corresponds to the {10 $\bar{1}$ 0} plane of hexagonal close-packed Ru [84]. The area along the perimeter of the crystalline nanoparticles is likely to be rich in the Ru–O bifunctional units required by our model for heterolytic hydrogen activation and ionic hydrogenation pathways.

The powder X-ray diffraction (XRD) pattern of the same 10 wt% catalyst (Fig. S2) was indistinguishable from that of the MgO support; no diffraction attributable to a Ru phase was evident, with all three peaks at $2\theta = 37.0^\circ$, 43.0° , and 62.4° assigned to MgO [85]. This indicates that the Ru phase in the Ru/MgO catalyst is nanocrystalline, without ordered structure over significant distances; RuNPs are thus highly dispersed and too small to be detectable by XRD, in agreement with the TEM results.

The elemental composition of Ru/MgO catalysts was analyzed by energy-dispersive X-ray spectroscopy (EDX) in a scanning electron micrograph (SEM). Fig. S3 contains the EDX spectra and corresponding elemental composition for all three carbon coated catalyst samples. The Ru content in the Ru/MgO catalysts is 10.1%, 5.1%, and 1.3%, for the nominal 10 wt%, 5 wt%, and 1 wt% catalysts, respectively, confirming the complete deposition of Ru onto MgO during catalyst syntheses.

In order to further investigate the nature of RuNPs on the catalyst surfaces, X-ray photoelectron spectroscopy (XPS) analysis was performed. Fig. S4 shows the full XPS spectra of fresh samples of different catalysts as well as of pure magnesia. While the presence of the C 1s peak is inevitable as carbonaceous species generally accumulate in the spectrometer chamber, the spectra show no detectable Cl (200 eV) or B (190 eV) species on the surface, confirming that the catalyst is free of contaminants from the preparation process. This represents an important advantage in terms of surface cleanliness in comparison with other preparation methods using RuCl₃ as precursor *e.g.* impregnation [86–88] and ion exchange [87], which usually lead to catalyst surfaces contaminated with chloride ions. The narrow scan for a 5 wt% Ru/MgO catalyst in the Ru 3d and 3p regions shown in Fig. 2a clearly indicates the

presence of metallic ruthenium on the MgO surface by the signals at 280.2, 460.8, and 483.2 eV, which correspond to Ru 3d_{5/2}, 3p_{3/2} and 3p_{1/2} spin–orbit components in the zerovalent state, respectively [89]; there is no evidence for the presence of other Ru species. Similar results were obtained for the 1 wt% and 10 wt% Ru/MgO catalysts. Interestingly, the spectrum of the 5 wt% Ru/MgO* (support prepared by us) displays a negative shift in the Ru 3d and 3p core level binding energies (Fig. 2b), as compared to the 5 wt% Ru/MgO (commercial support), suggesting a stronger metal–support interaction in the Ru/MgO* catalyst. This observation will be further discussed in the mechanistic section.

The specific surface areas of the magnesia support and of metallic Ru in the catalysts were determined by gas physisorption and chemisorption measurements, respectively, and the corresponding data are collected in Table 1. Commercial MgO has a specific (BET) surface area of 88 m² g^{−1} after calcination at 500 °C for 2 h, while the synthesized MgO* powder has a much larger surface area of 150 m² g^{−1}. The metallic surface area was determined by H₂ pulse chemisorption, and a typical profile is displayed in Fig. S5. The full coverage of exposed Ru surface by chemisorbed hydrogen atoms is indicated by the saturation of the hydrogen peak. Using a H/Ru_s = 1 stoichiometry [88], the Ru surface area can be calculated, from which the Ru dispersion and effective size of Ru crystallite can be derived. The 5 wt% and 10 wt% Ru/MgO catalysts share similar high metal dispersion (28% and 25%) and therefore very similar average size, as verified by TEM results. The 1 wt% catalyst, however, has a very low Ru dispersion (4%), probably because at such a low metal loading the majority of RuNPs penetrate into pore structures of MgO, leaving only a limited amount of Ru exposed on the catalyst surface. The effective crystalline sizes derived from H₂ chemisorption data are larger than those determined by TEM (see Table 1). These differences arise from the assumptions used in the calculation of particle size from chemisorption results, that the particles are spherical, and all metal surfaces are accessible, which is not true in practice. The shape of particles is not perfectly spherical, and importantly, the entire RuNP surfaces are not available as some particles are likely to be partially embedded on the surface while some reside in pore structures of magnesia.

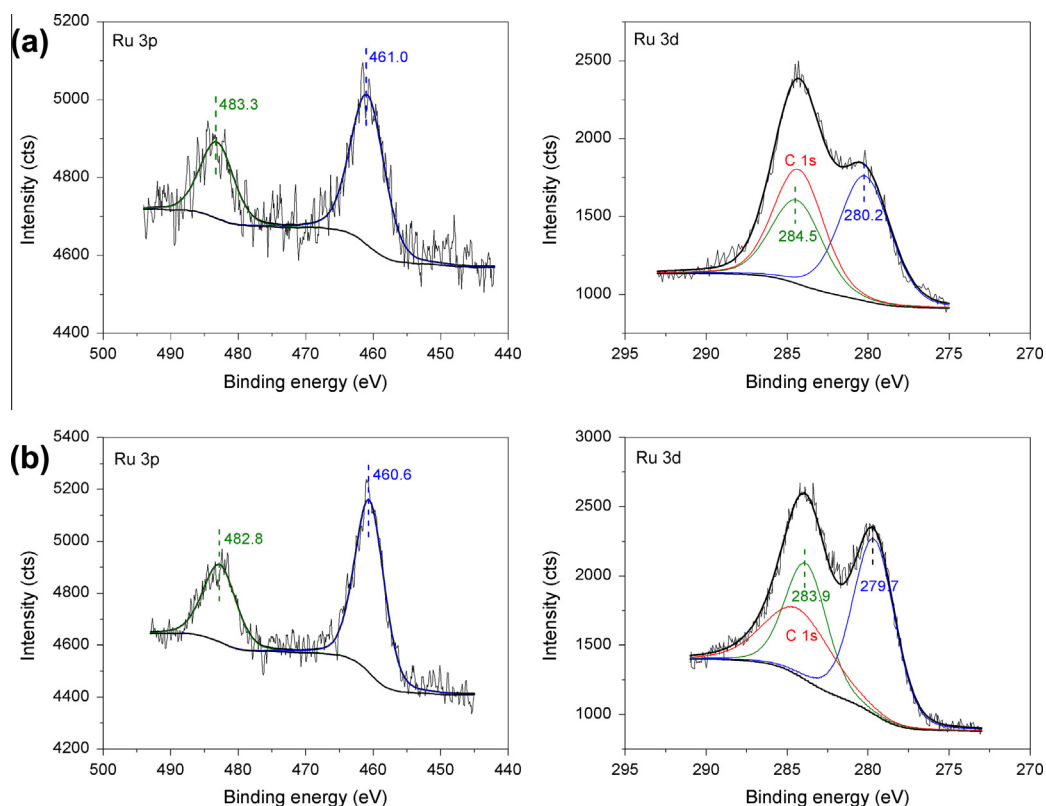


Fig. 2. XPS spectra (Al K α radiation) of (a) 5 wt% Ru/MgO and (b) 5 wt% Ru/MgO⁺ catalysts in the Ru 3d and 3p regions.

Table 1
Physical properties of magnesia supports and catalysts.

Material	Ru loading ^a	BET surface area (m ² /g) ^b	D _{H₂} ^c	\bar{d}_{H_2} (nm) ^d	d_{TEM} (nm)
MgO	–	88 ± 2	–	–	–
MgO ⁺	–	150 ± 20	–	–	–
1 wt% Ru/MgO	1.3%	–	4 ± 1%	35	1.5 ± 0.5
5 wt% Ru/MgO	5.1%	–	28 ± 3%	4.7	1.8 ± 0.5
5 wt% Ru/MgO ⁺	5.0%	–	22 ± 2%	6.0	1.8 ± 0.4
10 wt% Ru/MgO	10.1%	–	25 ± 1%	5.3	2.1 ± 0.6

^a Determined by EDX.

^b Single-point BET value.

^c Metal dispersion, determined by H₂ pulse chemisorption.

^d Effective particle size calculated from H₂ chemisorption results by $d_{H_2} = \frac{F}{\rho_{Ru} S}$ (F: crystallite geometry factor, 6 for hemisphere; S: active Ru surface area per g of Ru).

The basicity features of the MgO surfaces were evaluated by temperature-programmed desorption (TPD) using CO₂ as the probe molecule. The TPD profiles of the two magnesia supports and the corresponding 5 wt% catalysts display three CO₂ desorption peaks at approximately 100 °C, 180 °C, and 280 °C (Fig. S6), indicating the existence of a variety of basic sites of different strength on the surface of magnesia, which have been associated with O²⁻ sites with different coordination numbers [75]. The freshly prepared MgO⁺ displays a larger number of basic sites of each type in comparison with commercial MgO, as evidenced by the larger area under the corresponding curves. Deposition of RuNPs on the support necessarily diminishes the number of basic sites in both catalysts, as a proportion of them are likely to be occupied by metal particles stabilized through metal–oxygen interactions.

2.3. General considerations on catalytic hydrogenation

The catalytic activity of our Ru/MgO catalysts for the liquid-phase hydrogenation of a variety of aromatic compounds

representative of components of petroleum-derived fuels was tested in a batch reactor, monitoring the course of the reaction by periodically withdrawing samples and analyzing them by GC–MS. A composition profile as a function of time was generated for each aromatic substrate during hydrogenation, as exemplified in Fig. 3 for toluene (Tol) and quinoline (Q). Turnover frequency (TOF) values were obtained from the slopes of turnover number vs. time plots [90] and corrected for metal dispersion. Thus in this paper, unless otherwise specified, TOF is defined as the number of moles of substrate converted per mole of exposed surface Ru atoms per h.

The following control experiments were performed in order to establish the reliability of the hydrogenation data: (i) All hydrogenation runs were repeated at least twice to ensure reproducibility of the results; average TOF values are reported. (ii) Each batch of catalysts prepared was tested in a toluene hydrogenation run under a standard set of conditions (120 °C, 10 atm H₂) prior to use in other reactions; a high reproducibility of the results was observed (<5% variation), indicating that the preparation method employed provides homogeneity between different batches. (iii)

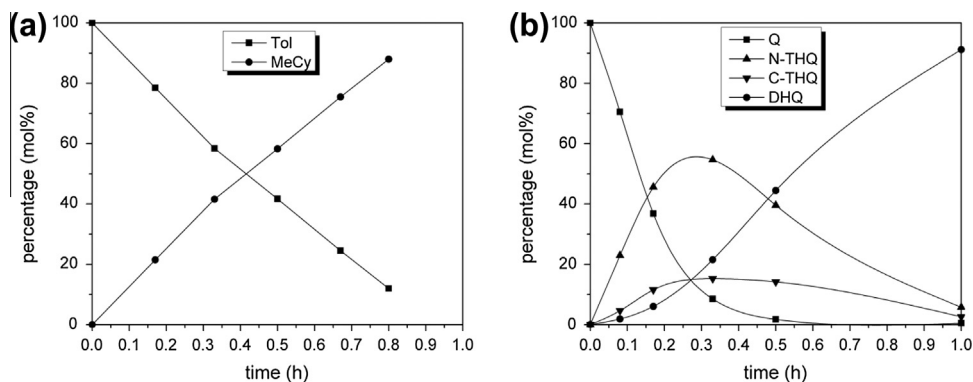


Fig. 3. Hydrogenation profiles for: (a) Toluene (1 mL; 100 mg 5 wt% Ru/MgO; in THF; 120 °C, 10 atm. Tol, toluene; MeCy, methylcyclohexane) and (b) Quinoline (1 mL; 100 mg 5 wt% Ru/MgO; in THF; 150 °C, 50 atm. Q = quinoline, N-THQ, 1,2,3,4-tetrahydroquinoline; C-THQ, 5,6,7,8-tetrahydroquinoline; DHQ, decahydroquinoline).

The reaction rates measured in a series of catalytic runs performed at different stirring speeds showed very little variation (<5%), indicating that mass transfer is not a rate-limiting factor. (iv) Blank tests employing MgO alone or in combination with NaBH₄ under reaction conditions analogous to those employed in the presence of the catalyst revealed no toluene or quinoline hydrogenation activity, thus excluding hydrogenation by any agents other than Ru/MgO. (v) After a neat toluene hydrogenation run under our standard conditions, the catalyst was separated from the liquid and the supernatant solution (>99% methylcyclohexane by GC-MS) was then tested for hydrogenation activity using *m*-xylene as the substrate. No hydrogenation products were detected by GC-MS after 1 h or 24 h reaction under constant hydrogen pressure, indicating that no metal leaching takes place under our experimental conditions.

2.4. Effect of metal loading and pressure

The effect of Ru loading and of hydrogen pressure on initial hydrogenation rates was studied using toluene (120 °C) and quinoline (150 °C) as model substrates in THF as solvent (see Fig. 4).

As expected, increased hydrogenation rates were observed for higher Ru loading for both Tol and Q, although the rate enhancement is not linear for Q (Fig. 4a); this difference in behavior can be related to the dual-site mechanism discussed in Section 2.7 below. Our data are consistent with a model involving two different types of active sites (A and B) for hydrogenation of toluene and quinoline; the different rate dependence on the metal loading for the two substrates indicates that the two distinct active sites operate through different kinetic regimes. With the data at hand, we

cannot provide a more detailed interpretation of this effect and a full kinetic analysis of these two reactions, which might further clarify the point, is outside the scope of this paper. From a practical point of view, the 5 wt% Ru/MgO catalyst seems the most adequate, and therefore, that metal loading was employed for most of the hydrogenation reactions discussed below.

Hydrogenation rates were found to steadily increase with increasing pressure for both toluene (10–30 atm) and quinoline (20–50 atm) (Fig. 4b), indicating that the Ru/MgO catalysts are stable against sintering or other metal aggregation processes at least up to 50 atm H₂, most likely due to strong interactions between the RuNPs and the surface oxygen sites. This agrees with the results of TEM measurements of the used Ru/MgO catalyst, as discussed in the previous section.

2.5. Substrate scope of hydrogenation reactions

In order to ascertain the scope of activity of the Ru/MgO catalyst, the hydrogenation of a series of aromatic hydrocarbons, as well as of N- and S-heteroaromatic compounds representative of components of petroleum-derived fuels, was carried out in liquid phase in a batch reactor.

2.5.1. Aromatic hydrocarbons

The data contained in Table 2 show that the Ru/MgO catalyst is highly active for hydrogenation of monocyclic and poly-cyclic aromatic hydrocarbons (MAHs and PAHs) under moderate temperature and pressure. The hydrogenation activity for MAHs decreases with increasing steric congestion on the arene rings, with the highest rate being observed for benzene and the lowest for mesitylene

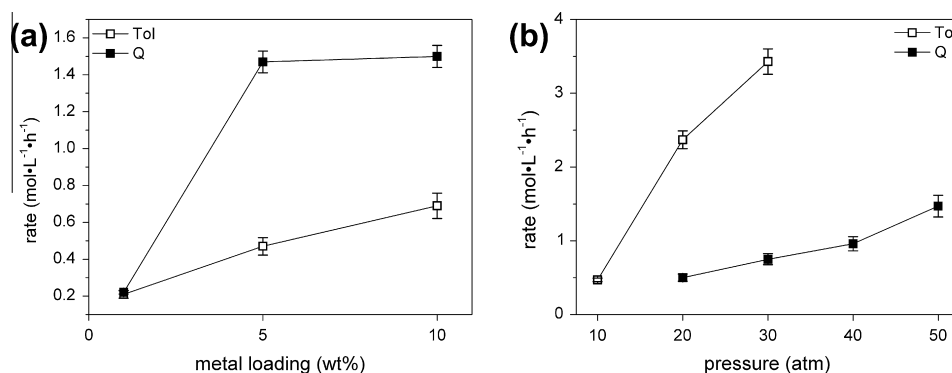


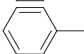
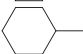
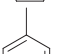
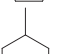
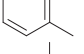
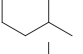
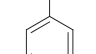
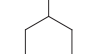
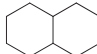
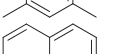
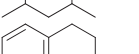
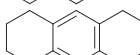


Fig. 4. Effect of (a) metal loading and (b) H₂ pressure on the rates of hydrogenation of toluene and quinoline (5 wt% Ru/MgO; 100 mg; substrates: 50 mmol; 120 °C for Tol and 150 °C for Q).

Table 2
Hydrogenation of MAHs and PAHs over 5 wt% Ru/MgO.

Entry	Substrate	Rate (mol L ⁻¹ h ⁻¹)	t _{1/2} (h)	TOF (h ⁻¹)	Product distribution at t _{1/2}
1 ^a		1.03	1.0	2300	 100%
2		0.47	1.5	1000	 100%
3		0.27	2.9	590	 100%
4		0.08	8.0	150	 100%
5 ^b		1.44	0.05	6600	 80%  15%
6		0.90	– ^c	4000	 75%  20%

^a Entries 1–4: liquid substrates, ~50 mmol; catalyst, 100 mg of 5 wt% Ru/MgO; n(sub):n(Ru) = 4000:1; 120 °C, 10 atm; in THF. In all tables, n(Ru) refers to moles of exposed surface Ru.

^b Entries 5–6: solid substrates, ~5 mmol; catalyst, 50 mg of 5 wt% Ru/MgO; n(sub):n(Ru) = 700:1; 150 °C, 50 atm; in THF; other minor products (<5%) are not listed.

^c No catalyst incubation; timing not started from the beginning of reaction.

(Table 2, entries 1–4). This is in agreement with previous finding on RuNPs in ionic liquids [38]. Poly-cyclic aromatics are generally more difficult to reduce and require increased temperature and pressure compared to monocyclic arenes; our Ru/MgO catalyst promotes the hydrogenation of naphthalene and anthracene with high TOF values of 6600 h⁻¹ and 4000 h⁻¹ at 150 °C and 50 atm, respectively (Table 2, entries 5 and 6).

Whereas monocyclic arenes were fully hydrogenated to the corresponding saturated hydrocarbons, naphthalene and anthracene were converted predominantly to the partially hydrogenated 1,2,3,4-tetrahydro products, at least over the half-life of the substrates.

This broad aromatic substrate scope of the Ru/MgO catalyst, combined with a high activity for PAHs, is notable. Other supported Ru catalysts have been shown to hydrogenate arenes, but most of the published work is concerned with benzene and other monocyclic arenes [42–45,47–58,62–64], with only very few examples available for PAHs [46,60,72].

2.5.2. N-heteroaromatic compounds

Nitrogen-containing compounds present in fuels are of great concern not only because they contribute to NO_x emissions but also because they commonly act as catalyst poisons. We find that our Ru/MgO catalyst is not only resistant to poisoning by a variety of common N-heteroaromatic compounds, but can efficiently hydrogenate them under moderate temperature and pressure, as summarized in Table 3. Mono-, bi-, and tri-cyclic N-heteroaromatics are hydrogenated with high TOF values ranging from 1000 h⁻¹ for indole (Table 3, entry 2) to 6000 h⁻¹ for acridine (Table 3, entry 6); the pyridine-based series is hydrogenated more easily than the pyrrole-based counterpart. Pyrrole and pyridine were exclusively reduced to pyrrolidine and piperidine (Table 3, entries 1 and 4), while poly-cyclic substrates yielded mixed products; quinoline and indole were hydrogenated predominantly at the N-heterocycle, with only a small fraction of the products resulting from hydrogenation of the carbocyclic rings (Table 3, entries 2 and 5). Apart from our Ru/PVPy catalyst [72], very few other supported Ru catalysts are known for hydrogenation of N-aromatics and they display much lower activity. Ru/Al₂O₃ was found inactive for hydrogenation of quinoline [91]; Ru on hydroxyapatite hydrogenates quinoline and its methylated derivatives with uncorrected TOFs in the range 50–150 h⁻¹ at 150 °C and 50 atm [59], while RuNPs on

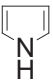
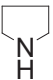
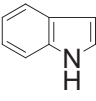
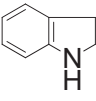
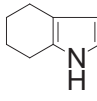
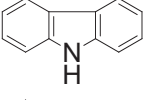
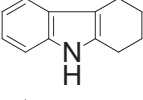
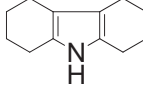
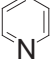
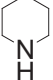
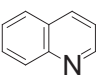
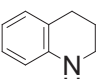
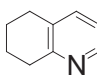
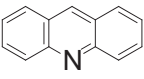
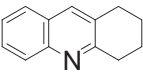
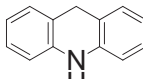
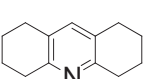
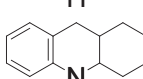
polydimethylphosphazenes promote the hydrogenation of quinoline and pyridine with uncorrected TOFs of about 200 h⁻¹ at 25 °C and 50 atm [60]; Ru/SiO₂ can reduce acridine and indole in addition to quinoline with uncorrected TOFs from 50 h⁻¹ to 200 h⁻¹ at 100 °C and 30 atm, to yield a mixture of products observed [46].

For hydrogenation of carbazole and its derivatives, alumina-supported Ru catalysts work under harsher conditions (130–150 °C, 70 atm) with uncorrected TOF values of about 400 h⁻¹ and 800 h⁻¹ for carbazole and 9-ethylcarbazole, respectively [65]; other RuNPs supported on different inorganic solid supports achieve uncorrected TOF values of about 3–5 h⁻¹ under 130 °C and 70 atm [66,67]. In contrast, the TOF values measured for our Ru/MgO catalyst are in the range 1000–6000 h⁻¹ (uncorrected values 300–1700 h⁻¹) in the hydrogenation of mono-/poly-cyclic N-heteroaromatics at 150 °C and 50 atm.

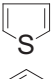
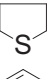
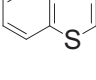
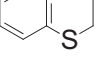
2.5.3. S-heteroaromatic compounds

Hydrogenation of S-heteroaromatics is the biggest challenge for supported noble metal catalysts due to the strong poisoning effect of the sulfur compounds. Indeed, there are very few examples in the literature regarding hydrogenation of S-heteroaromatics by use of noble metal NPs catalysts. RuNPs supported on silica failed to catalyze the hydrogenation of benzothiophene (BT) or dibenzothiophene (DBT) [46]; colloidal Rh suspensions stabilized by surfactants show no activity toward hydrogenation of thiophene (T) or BT [92]; metal oxide-supported Rh nanoparticles and Ru, Rh, Pt, Ir-based multimetallic nanoparticles achieved up to ~3% conversion of BT to 2,3-dihydrobenzothiophene (DHBT) after 24 h (uncorrected TOF ~0.1–0.2 h⁻¹) [93]. Table 4 summarizes the results of hydrogenating S-heteroaromatics using our 10 wt% Ru/MgO catalyst. At 200 °C under 50 atm H₂, Ru/MgO hydrogenates thiophene with an average TOF of 0.2 h⁻¹ (entry 1); BT is hydrogenated more rapidly (entry 2), with an average TOF of 1.0 h⁻¹ (uncorrected TOF 0.3 h⁻¹). Using a larger BT to Ru ratio (entry 3), BT was hydrogenated with an average TOF of 2.0 h⁻¹ (uncorrected value 0.5 h⁻¹), within the first 24 h, and complete conversion of BT was achieved after 12 d. These data indicate that although the hydrogenation rates for T and BT are much slower than those for N-aromatics under the conditions employed, the catalyst is not poisoned by BT. In addition to hydrogenation products, trace amounts of desulfurization products were also observed for both

Table 3
Hydrogenation of N-heteroaromatics over Ru/MgO.^a

Entry	Substrate	Rate (mol L ⁻¹ h ⁻¹)	t _{1/2} (h)	TOF (h ⁻¹)	Product distribution at t _{1/2}
1 ^b		1.60	0.7	3700	 100%
2 ^c		0.22	0.4	1000	 90%  10%
3 ^d		0.44	0.2	2000	 75%  20%
4		1.96	0.4	4400	 100%
5		1.47	0.7	3400	 92%  7%
6		1.34	0.05	6000	 46%  28%  12%  12%

^a 5 wt% Ru/MgO; 150 °C, 50 atm; in THF.^b Entries 1 and 5: liquid substrates, ~50 mmol; catalyst, 100 mg; n(sub):n(Ru) = 4000:1.^c Entries 2–4, 6: solid substrates, ~5 mmol; catalyst, 50 mg; n(sub):n(Ru) = 700:1.^d Entries 3, 5 and 6: other minor products (<5%) are not listed.**Table 4**
Hydrogenation of S-heteroaromatics over Ru/MgO.^a

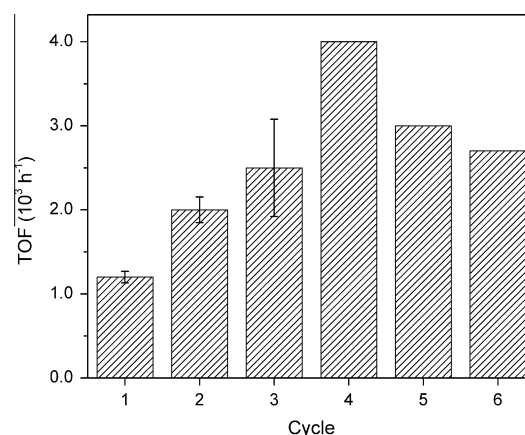
Entry	Substrate	Conv. (%) ^b	TOF (h ⁻¹) ^c	Products
1		11	0.2	
2		61	1.0	
3 ^d		23	2.0	

^a 100 mg of 10 wt% Ru/MgO, 200 °C and 50 atm, n(sub):n(Ru) = 40:1, in undecane.^b Conversion after 24 h.^c Average TOF over 24 h.^d Benzothiophene: 5.0 mmol, n(BT):n(Ru) = 210:1; conversion >95% at 12 d.

T (butenes/butane) and BT (ethylbenzene). Under similar reaction conditions, the more challenging substrates DBT and 4,6-DMDBT gave hydrogenation and desulfurization products only in GC-MS detectable trace amounts.

2.6. Catalyst recyclability and lifetime

The recyclability and lifetime of Ru/MgO was evaluated in six successive cycles of hydrogenation of neat toluene at 120 °C and 10 atm using the 10 wt% catalyst; the conversion was allowed to reach 100% in each cycle. As shown in Fig. 5, the catalyst displayed an enhancement of the activity after the first cycle, reaching a maximum around the fourth cycle. The total turnover number (TTO) for hydrogenation of neat toluene over the 10 wt% Ru/MgO catalyst, based on the six cycles of recycling experiments, is estimated to

**Fig. 5.** Activity (TOF) of 10 wt% Ru/MgO during recycling experiments.

be 120,000 but clearly this is not the limit, since the catalytic activity showed no decrease after the sixth cycle measured. Thus the Ru/MgO catalyst exhibits excellent recyclability and a long catalyst lifetime.

In an attempt to understand the rate enhancement observed during the first few cycles, additional measurements were undertaken. TEM images of 10 wt% Ru/MgO (Fig. S8) show no significant changes in average particle size or size distribution for a catalyst that was used twice, or six times, as compared to the freshly prepared catalyst. As noted in Section 2.3, the supernatant solution after a catalytic run did not display any hydrogenation activity, thus ruling out any metal leaching during the reaction. XPS data (Fig. S8) do not reveal any changes in the surface composition of

the catalyst, other than an increase in the C 1s peak, due to the accumulation of carbonaceous species from the reaction on the surface, which is normal for XPS spectra of used catalysts. These data confirm that the metal on the surface is stable under our reaction conditions.

One possible explanation for the activity enhancement observed during the first few cycles could be metal migration from the pores to the surface, which would result in an increase in the active metal surface area. However, the metal dispersion measured for the used catalyst was actually somewhat lower than that of the fresh catalyst, presumably because the residual surface carbon cannot be removed under the conditions of the hydrogen chemisorption measurements. Another possibility that we favor to explain the activity enhancement is related to the generation of an increasing number of active sites by prolonged contact with hydrogen and the substrate upon successive catalytic runs, until a maximum is achieved after about the third cycle.

2.7. Mechanistic implications

Our catalyst design aims at producing metal-base bifunctional units composed of RuNPs intimately associated with basic sites of the support to promote heterolytic activation of hydrogen and ionic hydrogenation mechanisms, as a strategy to avoid catalyst poisoning. We have previously presented evidence for such ionic hydrogenation pathways taking place over a Ru/PVPy catalyst, with the N atoms of the pyridine acting as the proton acceptors [72]. When magnesia is used as support, the surface O atoms of magnesia can function as strongly basic sites, as illustrated in Fig. 6. The Ru atoms along the perimeter of the nanoparticles (Fig. S2) must be in close proximity to surface oxygen atoms, thereby generating appropriate sites for heterolytic splitting of hydrogen (site A, Fig. 6). On the other hand, the Ru atoms on the bulk of the nanoparticles, away from surface O sites would behave as conventional metallic sites for homolytic splitting of hydrogen (site B, Fig. 6). Two different hydrogenation pathways may thus be operative in our hydrogenation reactions. A similar dual heterolytic/homolytic H₂ splitting capability was proposed for the reaction of unsupported RuS₂ with hydrogen, largely based on spectroscopic observation of surface Ru–H and S–H species [69].

To test the hypothesis of dual-site, dual-pathway mechanisms promoted by our Ru/MgO catalyst, substrate competition and thiophene selective inhibition experiments were conducted. Fig. 7a shows the results of hydrogenating an equimolar mixture of toluene and quinoline at 150 °C and 50 atm H₂. We note that during the early stage of reaction (first 15 min) quinoline was hydrogenated predominantly at the heterocyclic ring to yield 1,2,3,4-tetrahydroquinoline (N-THQ), and to a lesser extent at the carbocyclic ring to produce 5,6,7,8-tetrahydroquinoline (C-THQ). Interestingly, the initial rate of disappearance of quinoline in the mixture is identical to the one measured for quinoline alone (see comparison in

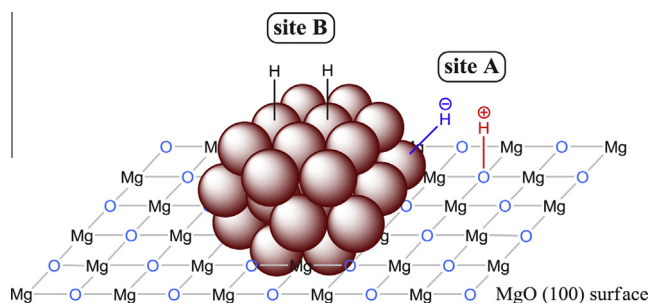


Fig. 6. The proposed dual-site structure of Ru/MgO catalyst illustrated by a Ru nanoparticle supported on the MgO surface.

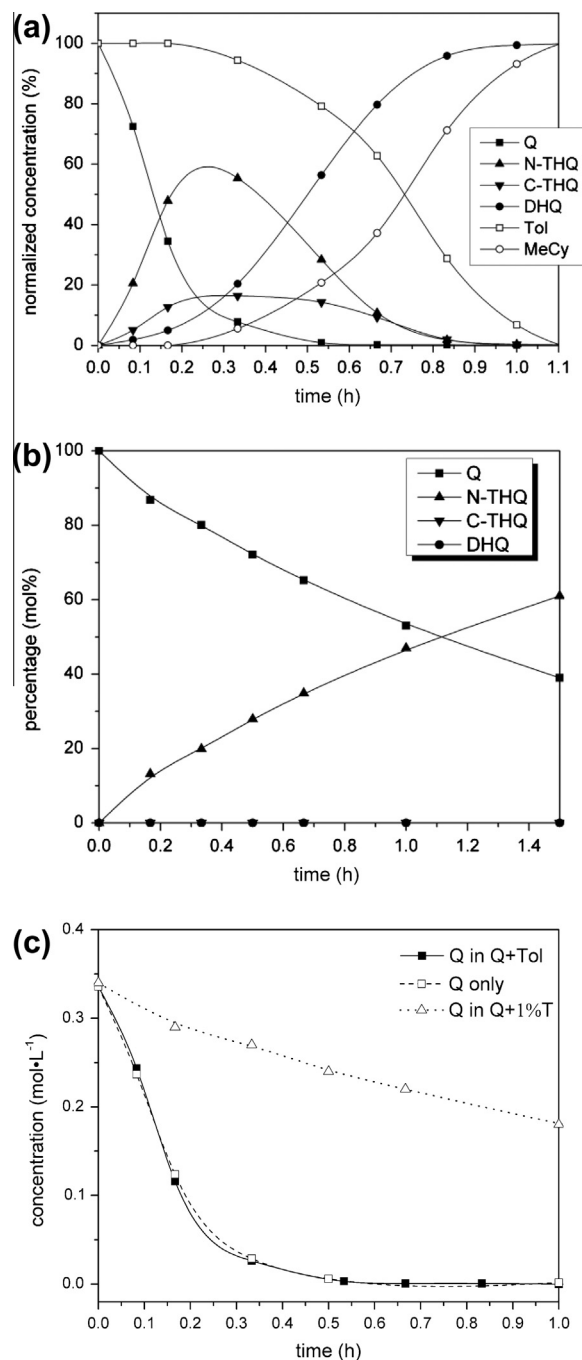
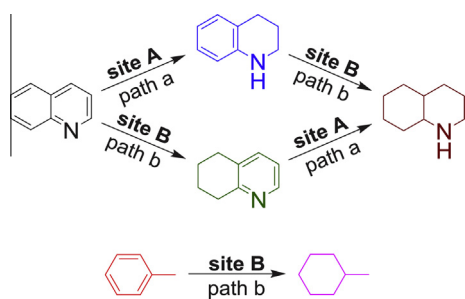


Fig. 7. (a) Substrate competition experiments: $n(Q):n(Tol):n(Ru) = 800:800:1$; in THF; 150 °C, 50 atm. (b) Selective thiophene inhibition experiment: $n(Q):n(T):n(Ru) = 800:5:1$; in THF; 150 °C, 50 atm. (c) Reaction profiles for hydrogenation of Q alone, Q + Tol (1:1), and Q + T (160:1).

Fig. 7c). However, hydrogenation of toluene in the mixture was essentially suppressed until most of the quinoline and N-THQ had been consumed, after which it proceeded at a significant rate.

When a quinoline hydrogenation run was carried out in the presence of a small amount of thiophene (~ 1 mol%), reduction of the carbocyclic ring was completely suppressed, whereas the N-heterocyclic ring was hydrogenated to yield N-THQ as the only product, albeit at a somewhat lower rate than the one observed for pure quinoline (Fig. 7c). The hydrogenation of pure toluene, in turn, was fully inhibited by the presence of thiophene. This implies that sites on the catalyst surface that would otherwise be



Scheme 2. Proposed dual-site mechanism for hydrogenation of Q and Tol on Ru/MgO.

available to adsorb arene rings are blocked by strong adsorption of thiophene, which is not transformed under these conditions (150 °C and 50 atm), but can be slowly hydrogenated at higher temperature (200 °C, Section 2.5.3).

All these observations point to a dual mechanism operating on two distinct types of active sites (Scheme 2). The N-heterocyclic and carbocyclic rings of quinoline are hydrogenated simultaneously, but with the latter at a lower rate; we postulate that the heterocyclic ring reacts at type A sites through an ionic route (path a) to produce N-THQ, while the carbocyclic ring is reduced on type B sites through conventional homolytic H₂ activation (path b) to form C-THQ. These parallel reactions block the access of toluene to the preferred B sites for carbocycles (path b), thereby suppressing its hydrogenation. Once most quinoline and N-THQ are consumed, toluene can effectively compete for type B sites and be hydrogenated. Thiophene binds preferentially to type B sites but has little affinity for type A sites, thus suppressing the hydrogenation of the carbocyclic ring of quinoline and of toluene, while having little effect on the hydrogenation of the heterocyclic ring of quinoline, ultimately yielding N-THQ as the only product.

To gain further insight into the hydrogenation mechanisms operating on the Ru/MgO catalyst, the hydrogenation of toluene and quinoline was also studied on the analogous Ru/MgO* catalyst. The MgO* support has a larger surface area than commercial MgO (Table 1) and a larger quantity of surface basic sites, as revealed by CO₂-TPD measurements (Fig. S6). The RuNPs deposited on MgO* with a metal loading of 5 wt% has essentially the same average particle size and size distribution as the 5 wt% Ru/MgO (see TEM image in Fig. S1c); the Ru content and dispersion of the 5 wt% Ru/MgO and Ru/MgO* are also similar (Table 1). However, the XPS spectrum of the Ru/MgO* catalyst showed a negative shift (~–0.5 eV) of Ru 3d and 3p core level binding energies as compared to Ru/MgO (Fig. 2b), implying a stronger metal-support interaction in the 5 wt% Ru/MgO* catalyst. Toluene is hydrogenated at approximately the same rates on both catalysts, while quinoline is hydrogenated much faster on Ru/MgO* than on Ru/MgO (Table 5). These observations are consistent with the dual-site mechanism proposed. Toluene is hydrogenated at type B sites, which we believe to be located on the bulk of the metallic nanoparticles, with little or no direct contact with the support; thus a similar activity is to be expected

for the two catalysts. On the other hand, the heterocyclic ring of quinoline is hydrogenated at type A sites, where we postulate heterolytic H₂ activation and ionic hydrogenation take place; a stronger Ru–O interaction in Ru/MgO* catalyst could be related to a higher number and efficacy of type A sites, leading to more efficient hydrogenation of quinoline, as shown by the data in Table 5.

3. Conclusion

We have prepared a series of catalysts composed of varying amounts of RuNPs supported on basic magnesium oxide and characterized them by a combination of TEM, EDX, PXRD, XPS, N₂ physisorption, H₂ pulse chemisorption and CO₂-TPD experiments. The RuNPs are well dispersed and stabilized on the support (mean size ~2 nm) and exist as crystalline particles in the zerovalent state. These materials proved to be versatile for the liquid-phase hydrogenation of a variety of mono- and poly-cyclic aromatic hydrocarbons, N-heteroaromatics, and S-heteroaromatics representative of components of petroleum-derived fuels, under moderate reaction conditions. They can be reused for several cycles without any appreciable loss of catalytic activity, reaching a TTO of at least 120,000 in the case of toluene. Through a combination of substrate competition and selective thiophene inhibition experiments, together with the observed effect of the magnesia support employed, we propose a catalytic mechanism involving heterolytic H₂ splitting and ionic hydrogenation pathways on the Ru/MgO surface for N-heterocycles, in addition to conventional homolytic H₂ activation and hydrogen transfer for carbocycles, and possibly S-aromatics. Such dual-site, substrate-dependent, dual-pathway mechanisms have interesting implications for future designs of new efficient and poison-resistant noble metal catalyst systems.

4. Experimental section

4.1. Materials

RuCl₃·3H₂O (Pressure Chemicals, Inc.) was used as received. Solvents (analytical grade, Sigma–Aldrich) were purified using a PureSolv purification unit from Innovative Technology, Inc. Substrates and other reagents (Sigma–Aldrich) were purified by distillation or recrystallization prior to use, as necessary. Naphthalene (≥99%, Sigma–Aldrich) was treated with AlCl₃ to remove trace amounts of benzothiophene before use. MgO (≥99%, ~325 mesh, Sigma–Aldrich) was calcined in air at 500 °C for 2 h and then stored in a desiccator for subsequent use.

4.2. Synthesis of Ru/MgO

The synthesis was performed in a three-neck round bottom flask fitted with two pressure-equalizing dropping funnels and a vacuum adapter. Using Schlenk techniques, the sealed apparatus was evacuated and purged with nitrogen three times. Under a nitrogen flow, MgO (1.0 g) was suspended in methanol (20 mL).

Table 5
Hydrogenation of toluene and quinoline over 5 wt% Ru/MgO and Ru/MgO*.^a

Substrate	Catalyst	Rate (mol L ⁻¹ h ⁻¹)	TOF (h ⁻¹)
	5 wt% Ru/MgO	0.47	1100
	5 wt% Ru/MgO*	0.50	1500
	5 wt% Ru/MgO	1.5	3400
	5 wt% Ru/MgO*	2.6	7500

^a Catalyst: 100 mg; substrate: 50 mmol; n(sub):n(Ru) = 4000:1; solvent: THF; 120 °C, 10 atm (Tol), 150 °C, 50 atm (Q).

The desired amount of $\text{RuCl}_3 \cdot 3\text{H}_2\text{O}$ (0.13 g; 0.5 mmol of Ru for 5 wt% Ru/MgO) in methanol (10 mL), and NaBH_4 (0.38 g, 10 mmol) in methanol (20 mL), were placed in the two dropping funnels, respectively. While the MgO suspension was being stirred at room temperature, 10 mL of the NaBH_4 solution was added to the flask, after which both RuCl_3 and NaBH_4 solutions were simultaneously added into the mixture at the same rate of about one drop per second. After addition was complete, the dropping funnels were removed and the mixture was stirred under N_2 at room temperature overnight. At the end, the solution was colorless and the solid was gray or dark. The solid was filtered off, washed with methanol (10 mL) six or more times until no Cl^- could be detected in the filtrate by use of AgNO_3 aqueous solution. The catalyst was dried under vacuum at room temperature, affording a fine gray to black powder, depending on the metal loading.

4.3. Catalyst characterization

4.3.1. TEM studies

Transmission electron micrographs were obtained on a JEOL JEM-2010 microscope operating at an accelerating voltage of 200 kV with a point-to-point resolution of 0.19 nm and magnification up to 1,500,000 \times . Images were captured digitally using an AMT Advantage CCD camera system (HRB Bottom Mount DVC Camera, 1 Megapixel) controlled by the AMT Image Capture Engine Software (Version 600.163) at varied high magnifications. The linear measurements on images had been calibrated previously at different high magnifications using known lattice spacing of crocidolite crystals standard ($d = 0.906$ nm) and graphited carbon crystals standard ($d = 0.34$ nm). TEM samples were prepared by placing a drop of catalyst suspension in THF on a holey carbon film coated copper grid and allowing evaporation of the solvent in the air. The particle size (Ferret diameter) distribution histogram was constructed from the measurement of about 300 particles found in representative images. The normal size distribution curve was also obtained based on the mean value and the standard deviation of the particle size.

4.3.2. Powder XRD measurements

Powder X-ray diffraction patterns were recorded on a Philips X'PERT MPD diffractometer using monochromatic $\text{Cu K}\alpha$ radiation ($\lambda = 1.5406$ Å) at 45 kV and 40 mA. Sample powder was placed in the holder with a flat surface and analyzed in air at room temperature. Spectra data were collected at a scanning rate of $0.10^\circ/\text{s}$ in a step size of 0.050° for 2θ over the range from 10° to 75° using the X'Pert Data Collector software (V. 2.2f). Phase identification was achieved by comparing the diffraction patterns of sample with that of ICDD (JCPDS) standards within the X'Pert HighScore software (V. 2.2c).

4.3.3. EDX analysis

The elemental composition of catalyst was assessed by energy-dispersive X-ray spectroscopy using a Zeiss Supra 55VP field emission scanning electron microscope equipped with an EDX detector. The samples were dispersed onto carbon tape and sputter coated with carbon before analysis. The spectra were acquired using the EDAX Genesis software, with an operating voltage at 15 kV and a working distance of 8.5 nm.

4.3.4. XPS analysis

X-ray photoelectron spectroscopy analysis was performed with an Omicron XPS spectrometer equipped with an EA125 multichannel hemispherical energy analyzer and a dual Al/Mg X-ray source using the monochromatic Al $\text{K}\alpha$ radiation (1486.6 eV). The binding energy scale was previously calibrated and the base pressure in the ultra-high-vacuum analysis chamber was around 2.0×10^{-9} torr.

The powdered samples were mounted on studs in air using a double-sided adhesive tape. Spectra recording was controlled by the EIS software (V. 2.2.4), using a scan step of -0.5 eV for survey scans and -0.1 eV for narrow scans. The binding energy scale was corrected for charging effect according to the position of Mg 2s photoelectron line (88.1 eV) [82,94]. The asymmetrical XPS peaks were deconvoluted by the curve fitting approach by use of XPSPEAK 4.1, applying Shirley background subtraction and Lorentzian-Gaussian functions (20% L, 80% G).

4.3.5. N_2 Physisorption, H_2 pulse chemisorption and CO_2 -TPD measurements

The BET surface area of support, the Ru surface area and CO_2 temperature-programmed desorption measurements were all conducted in a dual station Micromeritics Chemisorb 2750 analyzer fitted with a ChemiSoft TPx System. See Supporting Information for detailed experimental procedures.

4.4. Catalytic tests

Hydrogenation experiments were carried out using a 5513 Parr reactor (100 mL) fitted with an internal stirrer and a dip tube, a thermocouple, a sampling valve and a high-pressure buret, coupled to a 4836 controller. Reactions were performed in a glass liner placed inside the vessel of the reactor. In a typical hydrogenation run at 120°C and 10 atm, the reactor was loaded with the desired amount of catalyst and 20 mL of THF and then sealed. Hydrogen was introduced into the reactor through the high-pressure buret and released through the releasing valve; this was repeated three times in order to deoxygenate the system, after which the reactor was re-pressurized to 6 atm and heated to 120°C to reach ~ 10 atm. After the catalyst was incubated at 120°C and 10 atm for 1 h, 10 mL of substrate solution in THF was placed into the high-pressure buret, which was subsequently charged with 10 atm of H_2 . The reactor was depressurized to about 2–3 atm and the substrate solution in the buret was then quickly injected into the reactor; this was taken as the zero time of the reaction. The pressure was kept constant at 10 atm by feeding H_2 through an open connection to the hydrogen tank. Samples of the reaction mixtures were periodically withdrawn from the reactor and analyzed immediately by use of a Varian 3900 gas chromatograph fitted with a polar Supelco SP-2330 capillary column and a Saturn 2100T mass detector. The identity of each product was verified through comparison of its mass spectrum with the instrument's library and the molar percentage of each product was calculated based on peak areas and relative response factors previously determined by using standard solutions containing known amounts of each component. When necessary, samples were analyzed in a Shimadzu 2010 gas chromatographer fitted with a Restek Rtx-5 or Supelco SE-30 capillary column and an FID detector. Anthracene and sulfur compounds were added into the reactor together with catalyst from the beginning without catalyst incubation. Each experiment was repeated at least twice in order to ensure reproducibility; the variations in the calculated TOF values for repeat experiments were typically within 5%.

4.5. Recycling experiments and catalyst life time determination

About 100 mg of 10 wt% catalyst and 50 mL of neat toluene were placed in a glass liner inside the vessel of the reactor. The system was deoxygenated by flushing with H_2 three times. The reactor was first kept under 1 atm H_2 and then heated to 120°C ; after the temperature became stable, the reactor was pressurized to 10 atm, and this was taken as the zero time for the reaction. The pressure was kept constant during the whole reaction course. Samples were periodically withdrawn and the composition was

analyzed by GC–MS. The hydrogenation was left to run until 100% conversion was achieved. After the reactor was cooled down and the catalyst settled down to the bottom, methylcyclohexane (>99%) was simply withdrawn using a syringe fitted with a filter paper on the needle tip. Care was taken to minimize the loss of catalyst. The glass liner with the catalyst and some remaining methylcyclohexane was then placed into a large flask connected to a Schlenk line and the catalyst was dried under vacuum before being reused. This procedure was repeated six times.

4.6. Ruthenium leaching test

After the first cycle of hydrogenation of neat toluene during recycling experiments (Section 4.5), the reactor was cooled down and the catalyst was allowed to settle down to the bottom of the glass liner, after which the hydrogenated product methylcyclohexane (>99%) was carefully decanted and centrifuged. The supernatant liquid was then brought into a clean glass liner and 10 mL of fresh *m*-xylene was added; the liner was placed into the reactor and the conditions were adjusted to 120 °C and 10 atm H₂ in the same way as described in Section 4.5. No hydrogenation product of *m*-xylene was detected after 1 h or 24 h reaction through GC–MS analysis.

4.7. Substrate competition and selective thiophene inhibition experiments

The procedures for substrate competition and selective thiophene inhibition experiments are analogous to those described in the “Catalytic tests” section, except that the two substrates (toluene and quinoline in equimolar amounts), or substrate (toluene or quinoline) mixed with ~1 mol% thiophene were used, respectively.

Acknowledgments

This work was supported by the US Department of Energy through Grant DE-EE0003129. We thank the Environmental Sciences Analytical Center (ESAC) of Brooklyn College for access to the XRD and TEM instruments, Dr. Alan Lyons in the Chemistry Department of The College of Staten Island (CUNY) for use of the XPS instrument, and Dr. Jorge Morales in the Electron Microscopy Center of the City College of New York for assistance with EDX analyses.

Appendix A. Supplementary material

Supplementary data associated with this article can be found, in the online version, at <http://dx.doi.org/10.1016/j.jcat.2013.12.017>.

References

- [1] Trends in Renewable Energy Consumption and Electricity 2009, U.S. Energy Information Administration, Washington, DC, 2011.
- [2] Annual Energy Outlook 2010 with Projections to 2035, U.S. Energy Information Administration, Washington, DC, 2010.
- [3] World Energy Outlook 2010, International Energy Agency, Paris, France, 2010.
- [4] Regulation of Fuels and Fuel Additives, Code of Federal Regulations, Part 80, Title 40, 2011.
- [5] The California Reformulated Gasoline Regulations, California Code of Regulations, Sections 2250-2273.5, Title 13, 2008.
- [6] The California Diesel Fuel Regulations, California Code of Regulations, Sections 2281-2285, Title 13; Section 93114, Title 17, 2004.
- [7] European Commission, Directive 2009/30/EC of the European parliament and of the council of 23 April 2009 amending directive 98/70/EC as regards the specification of petrol, diesel and gas-oil and introducing a mechanism to monitor and reduce greenhouse gas emissions and amending council directive 1999/32/EC as regards the specification of fuel used by inland waterway vessels and repealing directive 93/12/EEC, OJ L 140 of 5.6.2009, pp. 88–113.
- [8] H. Topsøe, B.S. Clausen, F.E. Massoth, Hydrotreating catalysis, in: J.R. Anderson, M. Boudart (Eds.), *Catalysis Science and Technology*, vol. 11, Springer-Verlag, Berlin, 1996.
- [9] J. Ancheyta, J.G. Speight (Eds.), *Hydroprocessing of Heavy Oils and Residua*, CRC Press, Boca Raton, FL, 2007.
- [10] R.A. Sánchez-Delgado, *Organometallic Modeling of the Hydrodesulfurization and Hydrodenitrogenation Reactions*, Kluwer Academic, Dordrecht, 2002.
- [11] A. Stanislaus, B.H. Cooper, *Catal. Rev. Sci. Eng.* 36 (1994) 75–123.
- [12] G.C. Bond, *Catalysis by Metals*, Academic Press, New York, 1962.
- [13] V. Ponec, G.C. Bond, *Catalysis by metals and alloys*, in: B. Delmon, J.T. Yates (Eds.), *Studies in Surface Science and Catalysis*, vol. 95, Elsevier, Amsterdam, 1995.
- [14] G.C. Bond, *Metal-Catalysed Reactions of Hydrocarbons*, Springer, New York, 2005.
- [15] D. Astruc (Ed.), *Nanoparticles and Catalysis*, Wiley-VCH, Weinheim, Germany, 2008.
- [16] P. Serp, K. Philippot (Eds.), *Nanomaterials in Catalysis*, Wiley-VCH, Weinheim, Germany, 2013.
- [17] D. Astruc, F. Lu, J.R. Aranzas, *Angew. Chem. Int. Ed.* 44 (2005) 7852–7872.
- [18] A. Roucoux, J. Schulz, H. Patin, *Chem. Rev.* 102 (2002) 3757–3778.
- [19] J.A. Widegren, R.G. Finke, *J. Mol. Catal. A: Chem.* 191 (2003) 187–207.
- [20] A. Roucoux, *Top. Organomet. Chem.* 16 (2005) 261–279.
- [21] A. Gual, C. Godard, S. Castillon, C. Claver, *Dalton Trans.* 39 (2010) 11499–11512.
- [22] J.D. Scholten, B.C. Leal, J. Dupont, *ACS Catal.* 2 (2011) 184–200.
- [23] J.E. Mondloch, E. Bayram, R.G. Finke, *J. Mol. Catal. A: Chem.* 355 (2012) 1–38.
- [24] C. Amiens, B. Chaudret, D. Ciuculescu-Pradines, V. Colliere, K. Fajerweg, P. Fau, M. Kahn, A. Maisonnat, K. Soulantica, K. Philippot, *New J. Chem.* 37 (2013) 3374–3401.
- [25] P. Lara, K. Philippot, B. Chaudret, *ChemCatChem* 5 (2013) 28–45.
- [26] M. Zahmakiran, S. Ozkar, *RSC Green Chem. Ser.* 19 (2013) 34–66.
- [27] A. Gual, M.R. Axet, K. Philippot, B. Chaudret, A. Denicourt-Nowicki, A. Roucoux, S. Castillon, C. Claver, *Chem. Commun.* (2008) 2759–2761.
- [28] P.-J. Deboutiere, Y. Coppel, A. Denicourt-Nowicki, A. Roucoux, B. Chaudret, K. Philippot, *Eur. J. Inorg. Chem.* 2012 (2012) 1229–1236.
- [29] D. Gonzalez-Galvez, P. Nolis, K. Philippot, B. Chaudret, L.P.W.N.M. van, *ACS Catal.* 2 (2012) 317–321.
- [30] D. Gonzalez-Galvez, P. Lara, O. Rivada-Wheelaghan, S. Conejero, B. Chaudret, K. Philippot, L.P.W.N.M. van, *Catal. Sci. Technol.* 3 (2013) 99–105.
- [31] E. Rafter, T. Gutmann, F. Loew, G. Buntkowsky, K. Philippot, B. Chaudret, L.P.W.N.M. van, *Catal. Sci. Technol.* 3 (2013) 595–599.
- [32] A. Denicourt-Nowicki, A. Ponchel, E. Monflier, A. Roucoux, *Dalton Trans.* (2007) 5714–5719.
- [33] C. Hubert, A. Denicourt-Nowicki, A. Roucoux, D. Landy, B. Leger, G. Crowyn, E. Monflier, *Chem. Commun.* (2009) 1228–1230.
- [34] N.T.T. Chau, S. Handjani, J.-P. Guegan, M. Guerrero, E. Monflier, K. Philippot, A. Denicourt-Nowicki, A. Roucoux, *ChemCatChem* 5 (2013) 1497–1503.
- [35] M.V. Escárcega-Bobadilla, C. Tortosa, E. Teuma, C. Pradel, A. Orejón, M. Gómez, A.M. Masdeu-Bultó, *Catal. Today* 148 (2009) 398–404.
- [36] A. Nowicki, V. Le Boulaire, A. Roucoux, *Adv. Synth. Catal.* 349 (2007) 2326–2330.
- [37] E.T. Silveira, A.P. Umpierre, L.M. Rossi, G. Machado, J. Morais, G.V. Soares, I.J.R. Baumvol, S.R. Teixeira, P.F.P. Fichtner, J. Dupont, *Chem. – Eur. J.* 10 (2004) 3734–3740.
- [38] G.S. Fonseca, E.T. Silveira, M.A. Gelesky, J. Dupont, *Adv. Synth. Catal.* 347 (2005) 847–853.
- [39] M.H.G. Precht, M. Scariot, J.D. Scholten, G. Machado, S.R. Teixeira, J. Dupont, *Inorg. Chem.* 47 (2008) 8995–9001.
- [40] L.M. Rossi, G. Machado, *J. Mol. Catal. A: Chem.* 298 (2009) 69–73.
- [41] G. Salas, C.C. Santini, K. Philippot, V. Colliere, B. Chaudret, B. Fenet, P.F. Fazzini, *Dalton Trans.* 40 (2011) 4660–4668.
- [42] F. Su, F.Y. Lee, L. Lv, J. Liu, X.N. Tian, X.S. Zhao, *Adv. Funct. Mater.* 17 (2007) 1926–1931.
- [43] F. Su, L. Lv, F.Y. Lee, T. Liu, A.I. Cooper, X.S. Zhao, *J. Am. Chem. Soc.* 129 (2007) 14213–14223.
- [44] M. Takasaki, Y. Motoyama, K. Higashi, S.-H. Yoon, I. Mochida, H. Nagashima, *Chem. Asian J.* 2 (2007) 1524–1533.
- [45] G. Marconi, P. Pertici, C. Evangelisti, A.M. Caporusso, G. Vitulli, G. Capannelli, M. Hoang, T.W. Turney, *J. Organomet. Chem.* 689 (2004) 639–646.
- [46] C. Bianchini, V. Dal Santo, A. Meli, S. Moneti, M. Moreno, W. Oberhauser, R. Psaro, L. Sordelli, F. Vizza, *J. Catal.* 213 (2003) 47–62.
- [47] J. Huang, T. Jiang, B.X. Han, W.Z. Wu, Z.M. Liu, Z.L. Xie, J.L. Zhang, *Catal. Lett.* 103 (2005) 59–62.
- [48] J.B. Ning, J. Xu, J. Liu, F. Lu, *Catal. Lett.* 109 (2006) 175–180.
- [49] S. Boujday, J. Blanchard, R. Villanneau, J.-M. Krafft, C. Geantet, C. Louis, M. Breyse, A. Proust, *ChemPhysChem* 8 (2007) 2636–2642.
- [50] X. Zhou, T. Wu, B. Hu, T. Jiang, B. Han, *J. Mol. Catal. A: Chem.* 306 (2009) 143–148.
- [51] S. Niembro, S. Donnici, A. Shafir, A. Vallribera, M.L. Buil, M.A. Esteruelas, C. Larramona, *New J. Chem.* 37 (2013) 278–282.
- [52] M. Zahmakiran, S. Ozkar, *Langmuir* 24 (2008) 7065–7067.
- [53] M. Zahmakiran, T. Kodaira, S. Ozkar, *Appl. Catal. B* 96 (2010) 533–540.
- [54] M. Zahmakiran, Y. Tonbul, S. Ozkar, *Chem. Commun.* 46 (2010) 4788–4790.
- [55] M. Zahmakiran, Y. Tonbul, S. Ozkar, *J. Am. Chem. Soc.* 132 (2010) 6541–6549.
- [56] S. Miao, Z. Liu, B. Han, J. Huang, Z. Sun, J. Zhang, T. Jiang, *Angew. Chem. Int. Ed.* 45 (2005) 266–269.

- [57] G. Suss-Fink, B. Moollwitz, B. Therrien, M. Dadras, G. Laurency, A. Meister, G. Meister, *J. Cluster Sci.* 18 (2007) 87–95.
- [58] A. Denicourt-Nowicki, A. Roucoux, F. Wyrwalski, N. Kania, E. Monflier, A. Ponchel, *Chem. Eur. J.* 14 (2008) 8090–8093.
- [59] Y.-P. Sun, H.-Y. Fu, D.-L. Zhang, R.-X. Li, H. Chen, X.-J. Li, *Catal. Commun.* 12 (2010) 188–192.
- [60] A. Spitaleri, P. Pertici, N. Scalera, G. Vitulli, M. Hoang, T.W. Turney, M. Gleria, *Inorg. Chim. Acta* 352 (2003) 61–71.
- [61] R.A. Sanchez-Delgado, N. Machalaba, N. Ng-a-qui, *Catal. Commun.* 8 (2007) 2115–2118.
- [62] L. Song, X. Li, H. Wang, H. Wu, P. Wu, *Catal. Lett.* 133 (2009) 63–69.
- [63] S.O. Bin, R. Jothiramalingam, F. Adam, T. Radhika, T.M. Tsao, M.K. Wang, *Catal. Sci. Technol.* 2 (2012) 538–546.
- [64] K.X. Yao, X. Liu, Z. Li, C.C. Li, H.C. Zeng, Y. Han, *ChemCatChem* 4 (2012) 1938–1942.
- [65] F. Sotoodeh, K.J. Smith, *Ind. Eng. Chem. Res.* 49 (2010) 1018–1026.
- [66] K.M. Eblagon, D. Rentsch, O. Friedrichs, A. Remhof, A. Zuetzel, A.J. Ramirez-Cuesta, S.C. Tsang, *Int. J. Hydrog. Energy* 35 (2010) 11609–11621.
- [67] K.M. Eblagon, K. Tam, S.C.E. Tsang, *Energy Environ. Sci.* 5 (2012) 8621–8630.
- [68] C.A. Sandoval, T. Ohkuma, K. Muniz, R. Noyori, *J. Am. Chem. Soc.* 125 (2003) 13490–13503.
- [69] M. Breyse, E. Furimsky, S. Kasztelan, M. Lacroix, G. Perot, *Catal. Rev. Sci. Eng.* 44 (2002) 651–735.
- [70] R. Juarez, S.F. Parker, P. Concepcion, A. Corma, H. Garcia, *Chem. Sci.* 1 (2010) 731–738.
- [71] M. Frey, *ChemBioChem* 3 (2002) 153–160.
- [72] M. Fang, N. Machalaba, R.A. Sanchez-Delgado, *Dalton Trans.* 40 (2011) 10621–10632.
- [73] S. Ardizzone, C.L. Bianchi, B. Vercelli, *Colloid Surf. A – Physicochem. Eng. Asp.* 144 (1998) 9–17.
- [74] S. Ardizzone, C.L. Bianchi, B. Vercelli, *Appl. Surf. Sci.* 126 (1998) 169–175.
- [75] H. Hattori, *Chem. Rev.* 95 (1995) 537–558.
- [76] R. Rahi, M. Fang, A. Ahmed, R.A. Sanchez-Delgado, *Dalton Trans.* 41 (2012) 14490–14497.
- [77] A. Hornung, M. Muhler, G. Ertl, *Catal. Lett.* 53 (1998) 77–81.
- [78] A. Hornung, M. Muhler, G. Ertl, *Top. Catal.* 11 (2000) 263–270.
- [79] M.L. Kantam, R.S. Reddy, U. Pal, B. Sreedhar, S. Bhargava, *Adv. Synth. Catal.* 350 (2008) 2231–2235.
- [80] P. Moggi, G. Predieri, A. Maione, *Catal. Lett.* 79 (2002) 7–15.
- [81] J. Iwamoto, M. Itoh, Y. Kajita, M. Saito, K. Machida, *Catal. Commun.* 8 (2007) 941–944.
- [82] Y.V. Larichev, B.L. Moroz, V.I. Zaikovskii, S.M. Yunusov, E.S. Kalyuzhnaya, V.B. Shur, V.I. Bukhtiyarov, *J. Phys. Chem. C* 111 (2007) 9427–9436.
- [83] Q.C. Xu, J.D. Lin, X.Z. Fu, D.W. Liao, *Catal. Commun.* 9 (2008) 1214–1218.
- [84] Y. Zhang, D.F. Kang, M. Aindow, C. Erkey, *J. Phys. Chem. B* 109 (2005) 2617–2624.
- [85] Powder Diffraction File, Card # 65-0476, PDF-2/Release 2004, International Center for Diffraction Data, Newton Square, PA, USA.
- [86] V. Mazzieri, F. Coloma-Pascual, A. Arcoya, P. L'Argentiere, N.S. Figoli, *Appl. Surf. Sci.* 210 (2003) 222–230.
- [87] N. Kumar, P. Maki-Arvela, J. Hajek, T. Salmi, D.Y. Murzin, T. Heikkila, E. Laine, P. Laukkanen, J. Vayrynen, *Microporous Mesoporous Mater.* 69 (2004) 173–179.
- [88] J. Okal, M. Zawadzki, L. Kepinski, L. Krajczyk, W. Tylus, *Appl. Catal. A* 319 (2007) 202–209.
- [89] J.F. Moulder, W.F. Stickle, P.E. Sobol, K.D. Bomben, in: J. Chastain (Ed.), *Handbook of X-ray Photoelectron Spectroscopy: A Reference Book of Standard Spectra for Identification and Interpretation of XPS Data*, Perkin-Elmer, Eden Prairie, MN, 1992.
- [90] A.P. Umpierre, E. de Jesus, J. Dupont, *ChemCatChem* 3 (2011) 1413–1418.
- [91] M. Campanati, A. Vaccari, O. Piccolo, *J. Mol. Catal. A: Chem.* 179 (2002) 287–292.
- [92] V. Mevellec, A. Roucoux, *Inorg. Chim. Acta* 357 (2004) 3099–3103.
- [93] N.A. Beckers, S. Huynh, X. Zhang, E.J. Luber, J.M. Buriak, *ACS Catal.* 2 (2012) 1524–1534.
- [94] Y.V. Larichev, *J. Phys. Chem. C* 112 (2008) 14776–14780.